

## Construction and testing of the optical bench for LISA Pathfinder

This content has been downloaded from IOPscience. Please scroll down to see the full text.

2013 Class. Quantum Grav. 30 085006

(<http://iopscience.iop.org/0264-9381/30/8/085006>)

View [the table of contents for this issue](#), or go to the [journal homepage](#) for more

Download details:

IP Address: 194.94.224.254

This content was downloaded on 30/01/2014 at 12:59

Please note that [terms and conditions apply](#).

# Construction and testing of the optical bench for LISA Pathfinder

D I Robertson<sup>1</sup>, E D Fitzsimons<sup>1</sup>, C J Killow<sup>1</sup>, M Perreur-Lloyd<sup>1</sup>,  
H Ward<sup>1</sup>, J Bryant<sup>2</sup>, A M Cruise<sup>2</sup>, G Dixon<sup>2</sup>, D Hoyland<sup>2</sup>, D Smith<sup>2</sup>  
and J Bogenstahl<sup>3</sup>

<sup>1</sup> Institute for Gravitational Physics, School of Physics and Astronomy, SUPA,  
Glasgow University, Glasgow G12 8QQ, UK

<sup>2</sup> School of Physics and Astronomy, University of Birmingham, Edgbaston,  
Birmingham B15 2TT, UK

<sup>3</sup> Max Planck Institute for Gravitational Physics, Albert Einstein Institute, Callinstraße 38,  
D-30167 Hannover, Germany

E-mail: [david.robertson@glasgow.ac.uk](mailto:david.robertson@glasgow.ac.uk)

Received 19 December 2012, in final form 25 February 2013

Published 22 March 2013

Online at [stacks.iop.org/CQG/30/085006](http://stacks.iop.org/CQG/30/085006)

## Abstract

eLISA is a space mission designed to measure gravitational radiation over a frequency range of 0.1–100 mHz (European Space Agency *LISA Assessment Study Report* 2011). It uses laser interferometry to measure changes of order  $10 \text{ pm}/\sqrt{\text{Hz}}$  in the separation of inertial test masses housed in spacecraft separated by 1 million km. LISA Pathfinder (LPF) is a technology demonstrator mission that will test the key eLISA technologies of inertial test masses monitored by laser interferometry in a drag-free spacecraft. The optical bench that provides the interferometry for LPF must meet a number of stringent requirements: the optical path must be stable at the few  $\text{pm}/\sqrt{\text{Hz}}$  level; it must direct the optical beams onto the inertial masses with an accuracy of better than  $\pm 25 \mu\text{m}$ , and it must be robust enough not only to survive launch vibrations but to achieve full performance after launch. In this paper we describe the construction and testing of the flight optical bench for LISA Pathfinder that meets all the design requirements.

PACS numbers: 04.80.Nn, 06.30.Bp, 07.60.Ly, 07.87.+v, 42.82.Bq, 95.55.-n

(Some figures may appear in colour only in the online journal)

## 1. Introduction

The main aim of LPF is to demonstrate inertial free-fall of a test mass to a precision within an order of magnitude of that required for eLISA. This LPF goal is approximately two orders of



Content from this work may be used under the terms of the [Creative Commons Attribution-NonCommercial-ShareAlike 3.0 licence](https://creativecommons.org/licenses/by-nc-sa/3.0/). Any further distribution of this work must maintain attribution to the author(s) and the title of the work, journal citation and DOI.

magnitude better than demonstrated in any past spaceborne experiment. The mission consists of two free falling test masses housed inside a single drag free spacecraft. Laser interferometry is used to measure the changes in separation and angle between the two test masses, and also changes in separation and angle between the spacecraft and one test mass. The interferometry and readout is performed by the optical metrology subsystem (OMS). The mission is described in detail in [2].

## 2. Optical metrology subsystem

The OMS is the high resolution laser interferometry system that reads out the positions and angles of the test masses. It consists of four units, the reference laser unit (RLU), the laser modulator unit (LMU), optical bench interferometer (OBI) and the Phasemeter (PMU). The RLU is a Nd:YAG non-planar ring oscillator operating single mode at 1064 nm and at a power level of 40 mW. The LMU takes the laser light, splits it and passes each beam through an acousto-optic modulator. The beams are frequency shifted in one case by 80 MHz and in the other by 80.001 MHz resulting in two laser beams separated in frequency by 1 kHz. These beams are then directed onto the OBI. All of the optical connections between laser unit, modulator unit and optical bench are performed by single-mode, polarization-maintaining optical fibres.

On the OBI there are four heterodyne interferometers. Each interferometer combines two beams to produce an output signal at 1 kHz that is detected on quadrant photodiodes (QPD). The relative phases of these signals contain the interferometer output data and are measured by the PMU. Summing the signals from all four quadrants on one QPD gives a signal corresponding to path length changes between the two beams. The differential phase between opposite halves of the photodiode gives a differential wavefront signal (DWS) that corresponds to the relative angle between the two beams [3].

The reference interferometer is a static interferometer on the optical bench and provides the main phase reference. This signal is also used to stabilize the relative optical path length in the two optical fibres feeding light on to the OBI.

The frequency noise interferometer is another static interferometer on the optical bench. It has a path length difference between the two beams of 384 mm to enhance its sensitivity to laser frequency noise. This signal can then be used to actively stabilize the laser frequency or to allow laser frequency noise subtraction in post-processing.

The X1 interferometer measures the movement of test mass 1 relative to the optical bench and hence relative to the spacecraft since optical bench and spacecraft are rigidly connected. The X1 interferometer measures three degrees of freedom: movement along the  $x$ -axis and in the  $\phi$  and  $\eta$  angular directions. It is not first-order sensitive to test mass movement parallel to the  $y$ - $z$  plane or to roll in the  $\theta$  angular direction. The X12 interferometer is the main measurement interferometer; it measures the relative displacement between test mass 1 and test mass 2 and the relative angles between the two test masses in the  $\phi$  and  $\eta$  angular directions.

The layout of the OBI is shown in figure 1 and the reference frame in figure 2.

## 3. OBI requirements

The performance requirements for the OBI have been defined during an extensive system-level study of the overall mission. The details of this study and the resulting noise budget are not within the public domain, however the derived OBI specifications are presented here.

The principal requirement, set by the target test mass acceleration sensitivity for the mission, is that the OBI be able to monitor the relative displacement and angles between two test

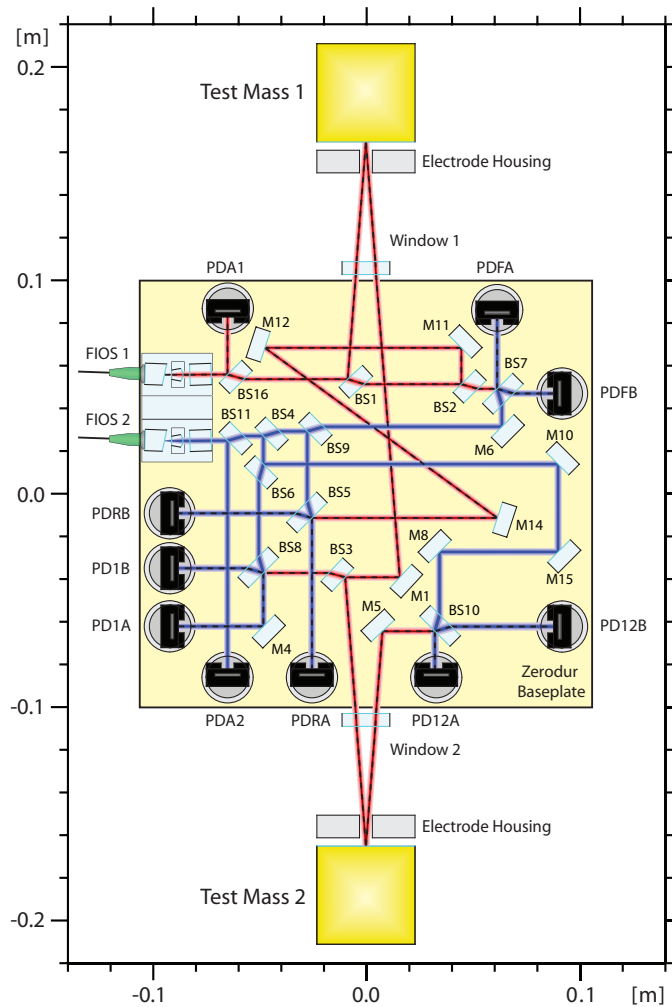


**Figure 1.** The OptoCAD [4] model of the OBI. Beam 1 (with the black dashed line) is the measurement beam and is reflected from both test masses, beam 2 is the reference beam which is confined to the optical bench.

masses in the frequency range 1–30 mHz with accuracies of  $6.3 \text{ pm}/\sqrt{\text{Hz}}$  and  $20 \text{ nrad}/\sqrt{\text{Hz}}$  respectively. This leads to a number of specific requirements detailed in the sections below. In addition there are also some general requirements related to operating in a space environment: the OBI must be able to survive launch vibration, radiation exposure, vacuum, and an operating temperature anywhere within the range 10–30°C. For robustness, mechanical stability and to minimize thermally driven effects, the OBI is based on a Zerodur<sup>®</sup> baseplate with fused silica components attached to it by hydroxide-catalysis bonding [5].

### 3.1. Alignment onto test masses

The LPF test masses are weakly electrostatically suspended in their housings and will have rotation noise of up to  $150 \text{ nrad}/\sqrt{\text{Hz}}$  in the measurement band. In order to keep the coupling

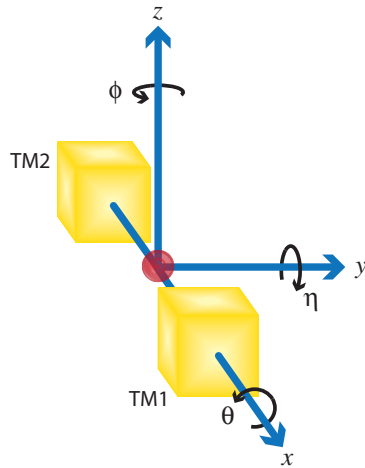


**Figure 2.** The reference frame for the OBI. The  $z$  axis is perpendicular to the surface of the OBI, with the  $x$ - $y$  origin centred on the OBI.

of test mass rotation to apparent longitudinal noise to an acceptable level the specification for the optical bench is that the optical beam should hit the nominal target points on the test masses with an absolute accuracy of better than  $\pm 25 \mu\text{m}$  in both  $y$  and  $z$ .

### 3.2. Interference quality

In order to maximize the output signal size, and to minimize the coupling of laser intensity and electronic noise sources, the optical beams should be well matched and aligned at the interference points. The system-level-determined requirement is that the optical contrast should be  $> 80\%$ . This cascades down to further requirements on specific beam parameters. In particular beam diameters should not differ by more than  $20\%$  and the wavefront curvatures ( $R_1$  and  $R_2$ ) should be matched so that  $|\frac{1}{R_1} - \frac{1}{R_2}| < 0.65 \text{ m}^{-1}$ . The polarization mismatch between the two beams should be less than  $11^\circ$ . These are principally requirements placed on the fibre injectors (see section 3.5).

Additionally, the positional and angular requirements are that the two interfering beams should be no further than  $140 \mu\text{m}$  apart, and with an angular misalignment of less than  $130 \mu\text{rad}$ . These, however, are rather loose requirements compared to the accuracy of beam alignment required to ensure proper pointing to e.g. the test masses, and so are automatically met (see section 4.2).

### 3.3. Photodiode alignment

All of the interferometers are read out by QPDs. These photodiodes have a  $45 \mu\text{m}$  gap between the quadrants. A small amount of the heterodyne signal is ‘lost’ in this gap. If one of the optical beams is angled with respect to the other and one of the beams is moving, then the phase of this ‘lost’ light will vary, causing an apparent longitudinal signal. This effect leads to a requirement that for LPF the photodiodes should be centred on the interfering beams to  $\sim \pm 33 \mu\text{m}$ .

### 3.4. Optical path length matching

In each interferometer there is an optical path length difference between beam 1 and beam 2. To minimize frequency noise coupling there is a requirement that the path length differences

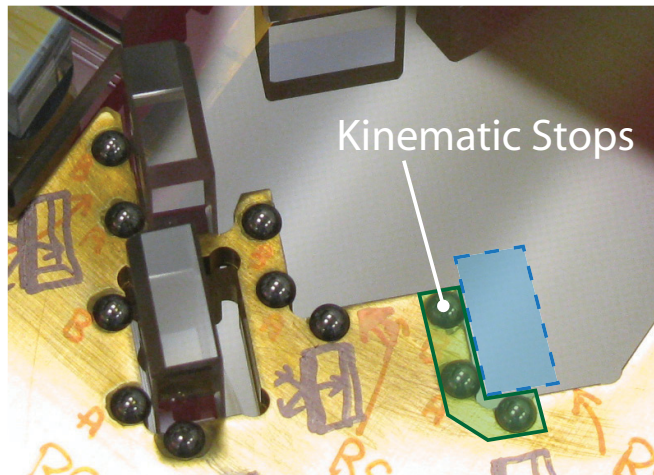


**Figure 3.** Template bonding showing two components already in place and the outline of where the third component will be placed against its kinematic stops. The two ball bearings behind the third component are 10 mm apart.

in the X1 and X12 interferometers should match that in the reference interferometer to better than 1 mm.

### 3.5. Fibre injector optical subassemblies (FIOS)

The two optical beams from the LMU arrive at the OBI in single-mode, polarization-preserving, optical fibres. Light from these fibres is matched to the mm diameter scale beams required on the OBI by custom designed, quasi-monolithic, fibre couplers (labelled FIOS in figure 1). The required alignment of beams onto the test masses imposes positioning and angular alignment constraints on the FIOS in the out-of-plane direction of  $\pm 20 \mu\text{m}$  and  $\pm 25 \mu\text{rad}$ .

## 4. OBI construction

All of the optical components are hydroxide-catalysis bonded to the OBI baseplate. In terms of alignment requirements there are two classes of components: those that can be placed and aligned with tolerances of order  $100 \mu\text{m}$  and  $4 \text{mrad}$ , and those that require the tightest possible tolerances of order  $10 \mu\text{m}$  and  $10 \mu\text{rad}$  [6]. The components with the less demanding tolerances are bonded to the OBI in groups of up to five. Their alignment is achieved by using precision engineered brass templates with steel ball-bearings to define the component positions (figure 3). The position of the template is aligned to the bench using precision screws, and its position verified with respect to the reference frame of the OB using a coordinate measuring machine (CMM)<sup>4</sup>.

The remaining components require higher precision alignment and are bonded individually. The component is positioned against ruby balls that are mounted on micrometer and piezo driven stages. The positions of these ruby balls are varied until the component is in the correct position and the component is then bonded in place (figure 4). One of two of

<sup>4</sup> The CMM used is a DEA Global Image 07.10.05 which, over a measurement baseline of  $L$  mm, has an uncertainty of  $(1.5 + 3.0 \times L/1000) \mu\text{m}$ .

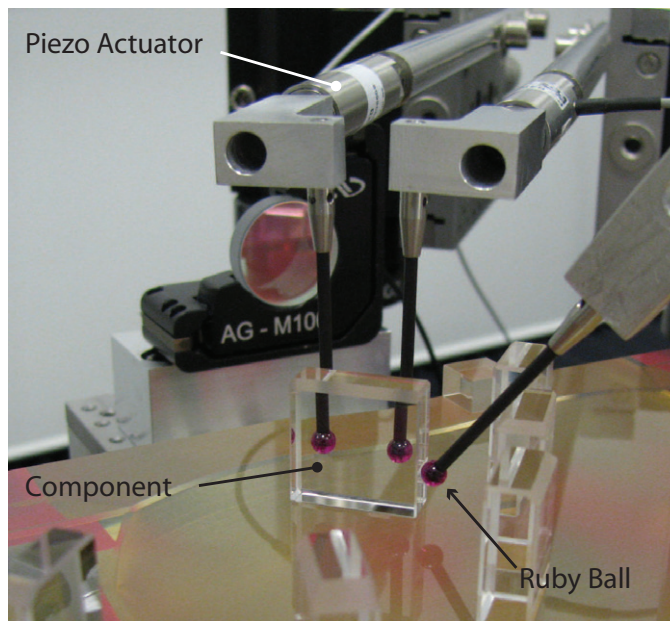


**Figure 4.** Precision bonding: the two actuators behind the component define the position and angle of the optical surface.

different methods is used to determine whether the component is in the correct position. In the first case, where the absolute vector of an optical beam has to be correct, a calibrated quadrant photodiode system (CQP) is used. The CQP consists of two QPDs and a beamsplitter mounted on a baseplate. The QPDs are mounted at different distances from the beamsplitter so that there is a unique optical beam that can be simultaneously centred on both QPDs. The CQP is calibrated so that the relationship between this unique optical vector and a mechanical reference frame on the baseplate is known. CMM measurements of both the OBI and the CQP allow the CQP to be positioned to any desired optical vector. The optical component can then be manipulated until the beam is centred on both QPDs. The CQP allows measurement of the beam position and angle with an accuracy of  $4\ \mu\text{m}$  and  $20\ \mu\text{rad}$  and is described in detail in [7]. In the second case, where the component is the final one in determining the heterodyne output, a simple QPD system with a 4-channel PMU is used. This allows the relative positions of the two beams to be measured using the relative power on the four quadrants, and the relative angles to be measured using the DWS signal. This approach yields accuracies of better than  $3\ \mu\text{m}$  and  $10\ \mu\text{rad}$  respectively in measurement of the relative beam position and angle.

The steps of the build are indicated in figure 5 and the relevant alignment methods given in table 1. The accuracies achieved in aligning and overlapping the heterodyne beams are given in table 2 and a photograph of the completed OBI is shown in figure 6.

#### 4.1. Alignments onto test masses

The alignment requirement of the beam on to test mass 1 is that it should be within  $\pm 25\ \mu\text{m}$  of its nominal position. In practice, provided the ‘as built’ alignment is known, any small offset in this alignment can be compensated when the OBI is mounted into the Pathfinder core assembly. The alignment on to test mass 1 will then be nominal, and the requirement

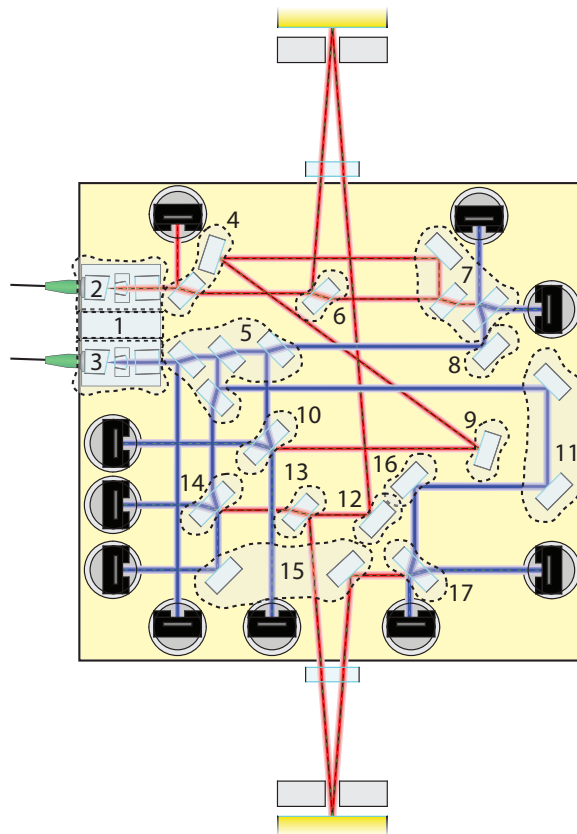


**Figure 5.** The steps in the overall build are sequentially numbered with dotted lines indicating the individual or group of components bonded at a particular step.

on the alignment on to test mass 2 is that it should be within  $\pm 50 \mu\text{m}$  of the actual beam position on test mass 1. The achieved deviations from nominal alignment at test mass 1 were  $(-6, -15) \mu\text{m}$  and  $(-16, -7) \mu\text{m}$  at test mass 2, each well within the  $\pm 25 \mu\text{m}$  requirement. The differential misalignment is  $(10, -8) \mu\text{m}$ , well within the  $\pm 50 \mu\text{m}$  requirement.

#### 4.2. DC positions, beam overlaps, contrast

Determinations of the relative alignment and position of the interfering beams at each interferometric detection point were made by a combination of beam vector measurements using the CQP and phase gradient measurements obtained using DWS. The results are shown in table 2.

#### 4.3. Photodiode alignment

The photodiodes are the final elements to be assembled on to the bench and have to be aligned on to the existing optical beams. The photodiode assembly is a two part structure consisting of a QPD in a titanium ‘cassette’ which mounts isostatically onto a titanium cruciform base. The base is glued onto the optical bench with an epoxy adhesive (Hysol EA 9361). This

**Table 1.** A table showing the alignment strategy for each of the bonding steps as defined in figure 5. All of the alignments apart from 2 and 3 (FIOS 1 and FIOS 2) are in-plane alignments. Heterodyne measurements align the beam overlap at the interference points of the interferometers. Calibrated Quadrant Photodiode pair (CQP) measurements were used for absolute position and angle measurements.

Step	Alignment method	What is controlled
1	Template	
2	Precision – CQP	Beam 1 out of plane angle and position
3	Precision – CQP	Beam 2 out of plane angle and position
4	Template	
5	Template	
6	Precision – CQP	Alignment onto test mass 1
7	Template	
8	Precision – Heterodyne	Frequency noise interferometer
9	Precision – CQP	Path length matching
10	Precision – Heterodyne	Reference interferometer
11	Template	
12	Precision – CQP	Path length matching
13	Precision – CQP	Alignment onto test mass 2
14	Precision – Heterodyne	X1 interferometer
15	Template	
16	Precision – CQP	Path length matching
17	Precision – Heterodyne	X12 interferometer

**Table 2.** The relative alignment of the optical beams at each of the measurement photodiodes. Note that although pairs of photodiodes look at complementary outputs of recombination beamsplitters they are at different distances from the beamsplitters so may have different offset values. Also shown is the optical contrast at each photodiode.

Photodiode	Displacement		Angle		Contrast (%)
	$x$ ( $\mu\text{m}$ )	$y$ ( $\mu\text{m}$ )	$\theta$ ( $\mu\text{rad}$ )	$\phi$ ( $\mu\text{rad}$ )	
PDRA	11	3	8	16	94
PDRB	11	7	8	16	94
PDFA	1	3	20	20	90
PDFB	1	1	20	20	90
PD1A	5	2	23	20	94
PD1B	4	2	23	20	94
PD12A	9	4	61	25	92
PD12B	3	5	62	26	92

arrangement allows the QPD to be removed and replaced while leaving the cruciform base on the optical bench. A thin glue layer ( $\gtrsim 100 \mu\text{m}$ ) avoids overstressing the Zerodur optical bench through thermal expansion of the titanium base while preserving good stability of photodiode positioning and alignment. All the glue layers thicknesses were in the range  $160\text{--}320 \mu\text{m}$ , which was within the requirements.

The alignment process starts by mounting the full photodiode structure onto a metal arm that allows adjustment in the plane of the photodiode surface. The photodiode mount is then measured by CMM. The whole structure is then clamped close to the optical bench and its position adjusted to centre the QPD onto the optical beam. The measurement of the position of the QPD is achieved by reading out the photocurrent from each quadrant of the QPD. This allows measurement of the position of the QPD relative to the optical beam to a precision of a few  $\mu\text{m}$ . Once the QPD is centred, a CMM measurement is taken to verify that the epoxy

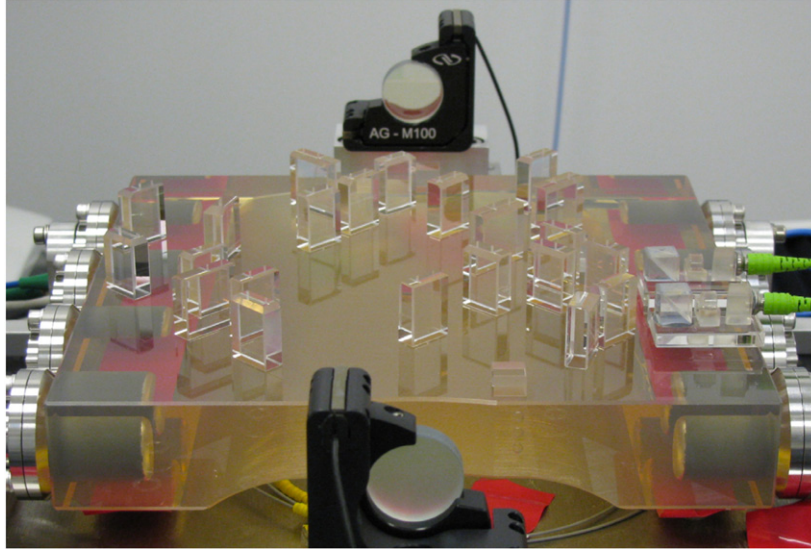


**Figure 6.** A picture of the completed OBI before the photodiodes were mounted. The FIOSs are on the right hand side. The black mirror mounts in the foreground and background hold mirrors in place of the test masses. The effect of the optical windows that the beams encounter passing to and from the real test masses is reproduced by appropriate location of the mirrors acting as test masses.

**Table 3.** Alignment accuracy of the QPDs. These are the errors relative to their optimal positions, all are within the requirement of  $\pm 33 \mu\text{m}$ . Measurement uncertainties are of order  $3 \mu\text{m}$ .

Photodiode	First fit		Second fit	
	$x (\mu\text{m})$	$y (\mu\text{m})$	$x (\mu\text{m})$	$y (\mu\text{m})$
PDRA	0	6	-2	-4
PDRB	-3	4	5	15
PDFA	1	-1	-11	-11
PDFB	3	10	22	-17
PD1A	-4	11	-2	-13
PD1B	-1	4	-14	-17
PD12A	3	12	-4	14
PD12B	-3	0	-19	24

layer will be of an acceptable thickness. If all is well, the QPD is removed, epoxy applied, and the QPD replaced on the bench. The precision achieved is shown in the ‘First fit’ column in table 3.

Unfortunately there were electrical problems with some of the QPDs and they all had to be removed and replaced. The realignment process for the replacement photodiodes was to mount the QPD cassette onto the existing cruciform base and read out the position of the optical beam on the QPD. The QPD cassette was then removed, adjusted and replaced and the process repeated until an adequate alignment was achieved. The alignments achieved after replacing the QPDs are shown in the ‘Second fit’ column in table 3.

#### 4.4. Optical path length matching

During the build the position of each beam was measured using the CQP and each optic was measured by CMM. From these measurements software ‘as-built’ optical (Optocad)

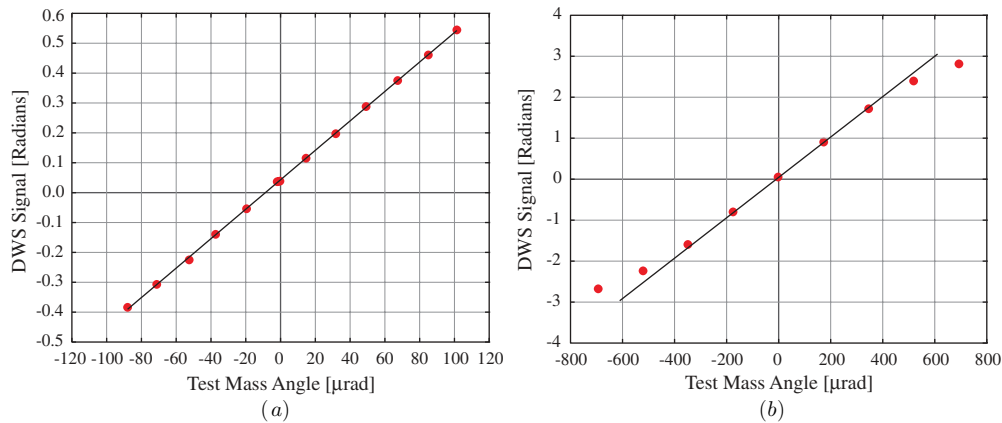


**Figure 7.** (a) DWS calibration over the full  $\pm 100 \mu$ rad operating range. The line is a linear fit to the measurement points (dots). (b) DWS signal over the full  $\pm 700 \mu$ rad capture range. The dots are the measured points and the line is the linear fit from the corresponding  $\pm 100 \mu$ rad operating range measurement. As expected the response becomes nonlinear when far from the operating point.

and mechanical (CAD) models of the bench were generated. The ‘as-built’ optical model was used as a tool to help optimize the path lengths during the build. The final model indicates that the achieved matching of the optical path length differences in the X1 and X12 interferometers to that in the reference interferometer is better than  $100 \mu\text{m}$ , well within the 1 mm requirement. Subsequent interferometric measurements (section 5.2) confirmed that the path length matchings were all within the 1 mm requirement.

## 5. Optical testing

### 5.1. DWS calibration

The DWS signals measure the angular orientation of the test masses and are used as error signals for the control of the test mass orientation. For optimal operation the DWS signal values at nominal test mass orientation, and the scaling factors as the test mass orientation changes, must both be obtained. Calibration is achieved by mounting a large (12 cm diameter) mirror on a hexapod [8] in place of the test mass. The position and angle of this mirror with respect to the optical bench is measured with the CMM and the DWS signals recorded. Repeated adjustments and measurements allow calibration over the full range of operating angles of both test masses. The large diameter mirror is required to maximize the precision of the angular measurement by the CMM.

DWS measurements were made over both the required linear operating range of  $\pm 100 \mu$ rad (figure 7(a)) and the results compared to those expected from optical modelling (table 4). DWS measurements were also taken over the capture range of the DWS system of  $\pm 700 \mu$ rad (figure 7(b)). The capture range is the angular range over which the DWS system is required to give a signal of the correct sign.

At test mass angles of up to  $0.5^\circ$  the relative power on each quadrant of the photodiodes can be used to estimate the test mass angle. The full range of this signal was explored (figure 8). One potentially important point to note from the relative power measurements is that as the beam approaches from far off the diode (i.e. during the acquisition phase), the dc signal does not rise monotonically but can vary in sign; this is shown in the inset in figure 8. This effect

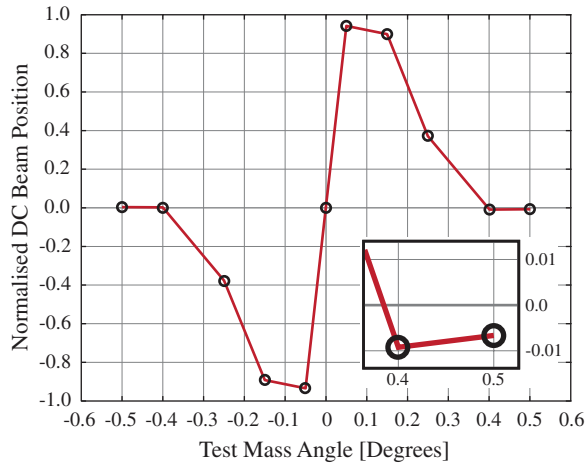


**Figure 8.** DC signal from QPD over large test mass tilt angles. As shown in the insert, at large test mass tilt angles the DC signal can unexpectedly change sign.

**Table 4.** Comparison of the measured DWS calibration factors with the predictions from the optical model. The maximum differences are  $< 10\%$  and are probably due to the small differences between the nominal beam parameters used for the model and the actual beam parameters in the real system. All numerical values are dimensionless: they are readout phase angle per test mass deviation angle.

Photodiode	In-plane		Out-of-plane	
	measured	model	measured	model
TM1 at PD1A	4960	4800	-4790	-4800
TM1 at PD1B	4980	4800	-4820	-4800
TM1 at PD12A	4590	4500	-4670	-4500
TM1 at PD12B	-4530	-4500	-4600	-4500
TM2 at PD12A	-5290	-5700	5180	5700
TM2 at PD12B	5160	5700	5310	5700

must be taken into account in the test mass acquisition phase as otherwise it will lead to a misinterpretation of the sign of the angular offset of the test mass which could then be driven further from its operating angle. The effect is almost certainly caused by effects internal to the photodiode cassette, e.g. reflections and scattering from the photodiode housing and internal wires bonded to the photodiode substrate. The effect here is observed with dummy test masses, it may change when the OBI is mounted in the spacecraft with real test masses and their attendant housings.

### 5.2. Optical path length matching

An experimental crosscheck of the path length matching was performed. The input laser light was frequency modulated and a comparison was made of the amplitudes of the resulting signals in the interferometer phase readouts. The measurement sensitivity was limited by the relatively noisy lab environment. A signal at the modulation frequency was seen only in the frequency noise interferometer, with no signal seen above the noise level in any of the other interferometers (figure 9). An upper bound to the path length mismatching of  $400 \mu\text{m}$  was deduced, confirming that the requirement had been met.

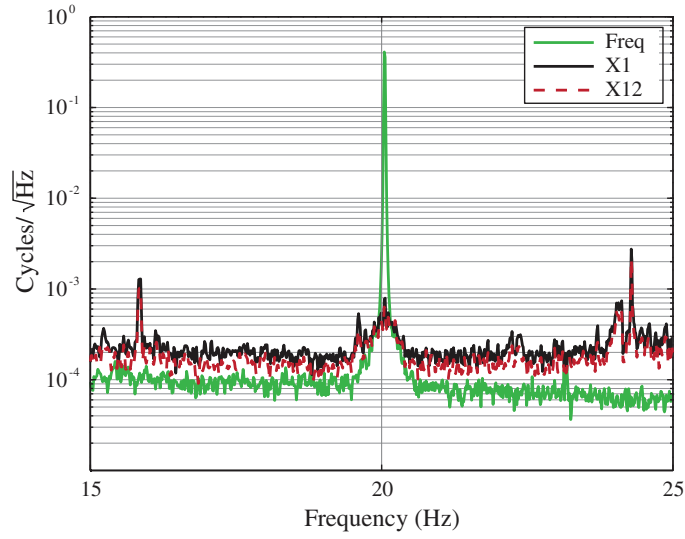


**Figure 9.** With a 20 Hz frequency modulation applied to laser, the relative prominence of the 20 Hz signal in the Frequency, X1 and X12 interferometers can be seen.

**Table 5.** Optical efficiency for beam 1 and beam 2. Note that this measurement was performed without dummy test masses present, so all the beam 1 light directed towards test mass 1 was detected and the subsequent photodiodes in the optical system were not illuminated. Uncertainties were estimated from the variations between repeated measurements in the same position.

Output port	Beam 1	Beam 2
	% of input light present	% of input light present
PDA1	7.2	–
PDA2	–	7.0
PDRA	8.5	9.2
PDRB	8.5	9.0
PDFA	8.4	8.3
PDFB	7.9	8.7
TM1	38.5	–
PD1A	–	8.9
PD1B	–	8.9
PD12A	–	10.2
PD12B	–	10.3
Total efficiency	$79.0 \pm 4$	$80.5 \pm 4$

### 5.3. Optical efficiency

One requirement for the OMS system is that the efficiency of the optical chain should be greater than 75%. The optical efficiency was measured before the final photodiodes were installed. A single moveable photodiode was used to measure the light power coupled in to the input fibres and the resulting power detected at the positions of the various photodiodes. The optical efficiency results were calculated from the relative power detected at the input and outputs and are given in table 5.

#### 5.4. Integrated optical testing

After completion of testing at the University of Glasgow the OBI was delivered to Astrium and integrated into a thermal optical qualification model (TOQM) of the complete OMS. The TOQM was used to undertake performance measurements under different configurations and operating scenarios. During these tests the longitudinal performance of the OMS reached its requirements and the angular performance (DWS) was substantially better than its requirements [9].

### 6. Conclusions

The flight model optical bench for LISA Pathfinder had to achieve a number of key requirements in terms of optical alignment and stability. We have described the building and testing of the optical bench showing how it has achieved or bettered all its requirements. Subsequent testing supervised by Astrium has shown that the longitudinal performance achieves its target sensitivity and the angular performance is substantially better than its requirements.

### Acknowledgments

The authors would like thank the entire international LPF team for many vigorous and useful discussions. We acknowledge financial support from SUPA, University of Glasgow, STFC, UKSA and ESA.

### References

- [1] *LISA Assessment Study Report 2011* (European Space Agency) ESA/SRE(2011)3
- [2] Racca G D and McNamara P W 2010 The LISA Pathfinder mission *Space Sci. Rev.* **151** 159–81
- [3] Morrison E, Meers B J, Robertson D I and Ward H 1994 Automatic alignment of optical interferometers *Appl. Opt.* **33** 5041–9
- [4] <http://home.rzg.mpg.de/~ros/optocad.html>
- [5] Elliffe E J, Bogenstahl J, Deshpande A, Hough J, Killow C, Reid S, Robertson D, Rowan S, Ward H and Cagnoli G 2005 Hydroxide-catalysis bonding for stable optical systems for space *Class. Quantum Grav.* **22** S257
- [6] Killow C J *et al* 2013 Construction of rugged, ultra-stable optical assemblies with optical component alignment at the micron level *Appl. Opt.* **52** 177–81
- [7] Fitzsimons E *et al* 2013 Precision absolute positional measurement of laser beams *Appl. Opt.* at press
- [8] [www.physikinstrumente.com](http://www.physikinstrumente.com)
- [9] Guzman F *et al* 2012 LISA technology package flight hardware test campaign *9th LISA Symp. (ASP Conference Series vol 467)* pp 141–50